LA-UR 06-3768
to be submitted to J. Acoust. Soc. Am.

Continuous thermoacoustic mixture separation

G. W. Swift and D. A. Geller

Condensed Matter and Thermal Physics Group,

Los Alamos National Laboratory,

Los Alamos, New Mexico 87545 *

(Dated: June 16, 2006)

Abstract

The superposition of nonzero time-averaged mole flux $\dot{N}$ on a thermoacoustic wave in a binary gas mixture in a tube produces continuous mixture separation, in which one or more partially purified product streams are created from a feedstock stream. Significant product and feedstock flows occur through capillaries that are small enough to experience negligible thermoacoustic phenomena of their own. Experiments with a 50–50 helium–argon mixture show diverse consequences of nonzero flow, involving the addition of only one simple term, $n_H\dot{N}$, to the equation for the heavy component's time-averaged mole flux, where n_H is the mole fraction of the heavy component. A boundary condition for n_H must be imposed on the equation wherever products flow out of the separation tube, but not where feedstock flows in.

PACS numbers: 43.35.Ud, 43.20.Mv, 43.35.Ty

I. INTRODUCTION

In thermoacoustic mixture separation, a sound wave propagating in a gas mixture in a tube causes one component of the mixture to flow in the sound-propagation direction and the other component to flow in the opposite direction.[1–3] The expenditure of acoustic power results in an increase in the Gibbs free energy of the mixture's components, and the energy efficiency of the process is comparable to that of some other practical separation processes.[4] Thermoacoustic separation is caused by oscillating radial thermal diffusion combined with oscillating axial viscous motion. The sound wave's oscillating pressure causes an oscillating radial temperature gradient, which in turn causes radial thermal-diffusion oscillations, inducing a small fraction of the light and heavy components of the mixture to take turns being partially immobilized in the viscous boundary layer near the tube wall. Thus, outside of that boundary layer, the sound wave's axial oscillating motion carries gas that is slightly enriched in the heavy component in one direction during half of the acoustic cycle and gas that is slightly enriched in the light component in the other direction during the other half of the cycle. In a 2-m-long tube, a 50–50 helium–argon mixture has been separated to yield 70% helium, 30% argon at one end and 30% helium, 70% argon at the other end; and a small enrichment of ^{22}Ne from natural neon has been demonstrated.[5]

The five papers cited above described some of the mathematical physics of this phenomenon. Analytical expressions for the radial dependences of oscillating temperature, density, mole fraction, and velocity and for the time-averaged molar separation flux were derived in the boundary-layer approximation, initially with no axial concentration gradient[1] and later with an arbitrary concentration gradient.[3] A numerical calculation was described that did not invoke the boundary-layer approximation.[3] Measurements confirmed the calculations,

initially with no axial concentration gradient in a tube where the boundary-layer approximation was adequate,[2] and later in a smaller-diameter tube with an axial concentration gradient.[3]

All of this theoretical work assumed that $\dot{N}_H + \dot{N}_L = 0$, where $\dot{N}_H$ and $\dot{N}_L$ are the time-averaged mole fluxes of the heavy and light components of the gas, respectively. In other words, it was assumed that the heavy and light mole fluxes were exactly equal in magnitude and in opposite directions. Similarly, all of the previous experimental work ensured that there was no bulk time-averaged total mole flux of the gas. In an engineering context, this corresponds to "batch" separation, in which a mixture is loaded into an apparatus, the apparatus is run for some time to accumulate an enriched product in one place and a depleted product in another place, and the products are finally removed. However, most industrial separation processes (e.g., petroleum refining, air separation, isotope enrichment[6–8]) run continuously, with feedstock steadily injected at one place while one or more enriched and depleted products are steadily removed elsewhere. Continuous separation requires nonzero total mole flux $\dot{N}$ superimposed on the separation flows, so that

$$\dot{N} = \dot{N}_H + \dot{N}_L \neq 0. \tag{1}$$

We undertook the work reported here to explore some fundamental aspects of continuous thermoacoustic mixture separation, for which inequality (1) is true.

Reference 3 showed that the first-order thermoacoustic momentum equation is unchanged by mixture-separation effects, and Doppler-shift effects are also negligible at the slow mean flows of interest here. Then the momentum equation shows that the evolution of the complex pressure amplitude p_1 with axial coordinate x is given by

$$\frac{dp_1}{dx} = -\frac{i\omega\rho_m/A}{1-f_\nu}U_1. \tag{2}$$

The evolution of the complex volume-flow-rate amplitude U_1 with x arises from the thermoacoustic continuity equation,[9] which can be expressed explicitly using Eq. (30) in Ref. 3 as

$$\frac{dU_1}{dx} = -\frac{i\omega A}{\rho_m a^2}\left\{1 + (\gamma - 1)\left[B f_\nu + C f_{\kappa D} + (1 - B - C) f_{D\kappa}\right]\right\} p_1. \tag{3}$$

In these equations and elsewhere, ω is the angular frequency, ρ_m is the mean density, a is the adiabatic sound speed, A is the cross-sectional area of the tube, and B, C, f_ν, $f_{\kappa D}$, and $f_{D\kappa}$ are defined in Ref. 3 and discussed in the Appendix here. Thus, we expect that the only change in the previous analysis caused by nonzero $\dot{N}$ is that Eqs. (41) and (44) of Ref. 3 should include an additional, convective term $n_H \dot{N}$, where n_H is the mean mole fraction of the heavy component. The combination of Eqs. (41) and (44) of Ref. 3 then shows that the mole flux of the heavy component is

$$\begin{aligned} \dot{N}_H \;=\; & n_H \dot{N} + \frac{\delta_\kappa}{4 r_h}\frac{\gamma - 1}{\gamma}\frac{k_T}{R_{\text{univ}} T_m}\,|p_1|\,|U_1|\,(F_{\text{trav}}\cos\theta + F_{\text{stand}}\sin\theta) \\ & + \frac{\delta_\kappa}{4 r_h}\frac{\rho_m |U_1|^2}{m_{\text{avg}}\omega A} F_{\text{grad}}\frac{dn_H}{dx} - \frac{\rho_m}{m_{\text{avg}}} A D_{12}\frac{dn_H}{dx}. \end{aligned} \tag{4}$$

The first term represents the mole flux of the heavy component that simply accompanies nonzero bulk flow of the gas mixture. The second term represents the thermoacoustic mixture-separation process described qualitatively above, which can cause the heavy component to flow in either direction with respect to its concentration gradient. The third term represents a qualitatively similar process of oscillating radial mass diffusion and axial viscous motion, but one that always works to reduce the magnitude of a nonzero concentration gradient. The fourth term represents ordinary axial mass diffusion, which also always works to reduce the concentration gradient. In Eq. (4) and throughout this paper, $\delta_\kappa = \sqrt{2k/\omega\rho_m c_p}$ is the thermal penetration depth, k is the thermal conductivity, c_p the isobaric specific heat, r_h is the hydraulic radius of the separation tube (for a circular tube, r_h is half of

the circle's radius R), γ is the ratio of isobaric to isochoric specific heats, k_T is the molar thermal-diffusion ratio, $R_{\rm univ} = 8.314$ J/mol-K is the universal gas constant, T_m is the mean temperature, θ is the phase by which p_1 leads U_1, $m_{\rm avg} = n_H m_H + (1 - n_H) m_L$ is the average molar mass, m_H and m_L are the heavy and light molar masses, respectively, and D_{12} is the binary mass-diffusion coefficient. The three real variables $F_{\rm trav}$, $F_{\rm stand}$, and $F_{\rm grad}$, which are generally < 0, depend on the properties of the gas and the local geometry of the tube. Analytical expressions for the three F's have been published previously in the boundary-layer limit,[1,3] but in the Appendix here we present analytical expressions for the F's in small circular tubes for the first time. The coupled differential equations (2), (3), and (4), with the expressions for the three F's given in the Appendix, have been implemented in the computer code DeltaE,[10] which has been used to create all the calculated curves in the figures below. In that implementation, Eq. (4) is solved for dn_H/dx and is integrated with respect to x simultaneously with Eqs. (2) and (3) to obtain $p_1(x)$, $U_1(x)$, and $n_H(x)$. The mole fluxes $\dot{N}$ and $\dot{N}_H$ are taken to be independent of x except where feedstock is injected or product is removed.

To solve Eqs. (2), (3), and (4) for $p_1(x)$, $U_1(x)$, and $n_H(x)$, boundary conditions on those three variables must be imposed. The boundary conditions for p_1 and U_1 are the same as for ordinary acoustics in tubes, but boundary conditions for n_H are less familiar. In batch separations, the number of moles of each gas in the apparatus at the end of the separation process is the same as at the beginning, so n_H must satisfy

$$\int n_H(x)\ dV = n_{H,\ \rm batch} V, \tag{5}$$

where $n_{H,\ \rm batch}$ is the initial heavy mole fraction of the batch and V is the volume of the apparatus. Continuous separations impose different constraints. In a capillary connected to

the separation tube at $x = x_o$ through which a product is removed continuously and which is small enough in diameter that acoustics within it is insignificant and the concentration gradient is zero, Eq. (4) is simply $\dot{N}_{H,\text{ product}} = n_{H,\text{ product}}\dot{N}_{\text{product}}$. The value of $n_{H,\text{product}}$ in that capillary must equal the local value in the separation tube where the capillary is connected. If the product is removed at an end of the separation tube, $\dot{N}$ and $\dot{N}_H$ in the capillary must also equal their values in the separation tube. Thus, the boundary condition imposed on n_H at an end x_o of the separation tube where a product is removed is simply

$$\dot{N}_H(x_o) = n_H(x_o)\dot{N}(x_o). \tag{6}$$

(If product were removed somewhere in the middle of the separation tube, the corresponding boundary condition would be

$$\dot{N}_H(x_o^-) - \dot{N}_H(x_o^+) = n_H\left[\dot{N}(x_o^-) - \dot{N}(x_o^+)\right].) \tag{7}$$

The algebraic simplicity of the boundary condition given in Eq. (6) disguises at least two interpretations. At the simplest level, Eq. (6) expresses "what goes in must go out" with respect to the region of the separation tube adjacent to the product-removal capillary's entrance. However, Eqs. (4) and (6) together show that the last three terms in Eq. (4) must sum to zero at such a location. This shows that the boundary condition can also be interpreted as a complicated local constraint relating dn_H/dx (which appears explicitly in two of those three terms) to n_H itself (on which most of the variables in all three terms depend implicitly).

In contrast to continuous product removal, continuous feedstock injection does not impose any explicit boundary condition on the solution to Eqs. (2), (3), and (4) in the separation tube. The total injection flux $\dot{N}_{\text{feedstock}}$ and the injection flux of the heavy component, $n_{H,\text{ feedstock}}\dot{N}_{\text{feedstock}}$, add to any time-averaged flows already in the separation tube and

compete with the terms of Eq. (4) and boundary conditions imposed elsewhere to determine the local value of n_H, which is not necessarily equal to $n_{H,\,\mathrm{feedstock}}$. If the feedstock capillary had a large enough diameter to support internal thermoacoustics, continuity of n_H at the junction of the capillary and the separation tube would presumably hold. As its diameter was reduced, dn_H/dx at the end of the capillary would steepen, eventually developing what we conveniently treat as a discontinuity here.

The verification of the presence of the first term in Eq. (4), $n_H\dot{N}$, and the boundary condition on n_H expressed in Eq. (6) are the principle quantitative goals of this work. The experiments described below used a helium–argon mixture in a loudspeaker-driven traveling-wave separation tube. Fed with a 50–50 mixture, concentrations at the ends of the tube ranged from 30% to 70%. Feedstock was added and products were removed via capillaries, small enough in diameter to eliminate significant internal thermoacoustic effects but large enough to allow steady flow without requiring high pumping power. Feeding gas to the middle of the separation tube and extracting products at both ends allows simultaneous continuous production of helium-enriched gas and argon-enriched gas. Feeding gas to one end and removing an almost equal amount from the same end allows continuous production of a single more-highly enriched gas at the other end. Measurements under both circumstances provide quantitative confirmation of the $n_H\dot{N}$ term in Eq. (4) and of the boundary condition expressed by Eq. (6).

II. APPARATUS AND INSTRUMENTATION

Figure 1 illustrates the apparatus we used to investigate these issues. The stainless-steel separation tube was 1 m long and had a 3.3-mm inside diameter. Near one end, access

through a valve and a very short, 1-mm-i.d. passage allowed rapid evacuation and addition of the gas mixture before each experimental run, to a mean pressure $p_m = 80$ kPa that was measured with a high-accuracy capacitance manometer[11] that had been checked recently against a mercury manometer. At each end of the tube was a bellows-sealed piston epoxied to the face of a loudspeaker. These two driver assemblies were used to maintain the sound wave in the gas, and are described more fully in Ref. 5. They were driven sinusoidally at 200 Hz by two phase-locked signal generators and audio amplifiers. Three piezoresistive pressure transducers[12] and a lock-in amplifier[13] were used to observe the resulting complex pressure amplitude p_1 in the gas at the ends and middle of the separation tube. Table I summarizes the important dimensions of the apparatus discussed above and other variables that are discussed later.

The heavy mole fraction n_H in the separation tube could be measured at the seven locations that are shown in Fig. 1. At each location, a microcapillary[14] continuously withdrew gas from the separation tube at a rate of $\sim 3 \times 10^{-10}$ mol/s. All seven microcapillaries were 5 cm long and nominally 10 μm inside diameter. These fragile microcapillaries were epoxied into larger copper tubes to protect against accidental damage. We found that two of them, henceforth referred to as the "large" microcapillaries, had 30% lower flow impedances than the other five, so the inside diameters of those two may have been 7% larger than the other five. The helium and argon flowing through the microcapillaries were detected by a computer-controlled, quadrupole-type residual gas analyzer[15] (RGA) pumped by a turbopump,[16] the latter backed by an oil-free mechanical pump.[17] A network of bellows valves allowed any of the seven microcapillaries to be connected to the RGA–pump system, which maintained the pressure at $\sim 10^{-6}$ torr in the presence of such flow. Meanwhile, the other six microcapillaries were connected to a second turbo pump and second mechanical

pump, to maintain high vacuum in all connecting tubing so that opening a valve never dumped a large amount of accumulated gas into the RGA. A measurement of n_H at a single microcapillary involved opening and closing the valves appropriately, waiting 2 minutes for steady state, and then averaging the RGA mass-4 and mass-40 "partial pressures" for 3 minutes. This averaging time yielded roughly 1% statistical uncertainty in the supposed ratio of mass-4 partial pressure to mass-40 partial pressure.

However, obtaining n_H from that "partial pressure" ratio was complicated because the RGA is much more sensitive to argon than to helium and because the RGA–pump system's response is slightly nonlinear,[18] with the nonlinearity being different for mass 4 and mass 40. We mapped out this complexity by recording the RGA's reported partial pressures for known helium–argon mixtures, which we prepared from the pure gases in a two-liter fan-stirred mixing chamber. These mixtures, ranging in concentration from 35–65 to 65–35, were forced through one small and one large microcapillary with 80-kPa pressure. The RGA results were slightly different for the partial pressures resulting from the large and small microcapillaries. We found

$$\left(\frac{pp_4}{pp_{40}}\right)_{\text{true}} = C_L \left(\frac{pp_4}{pp_{40}}\right)_{\text{RGA}}, \text{ large microcapillaries;} \tag{8}$$

$$\left(\frac{pp_4}{pp_{40}}\right)_{\text{true}} = C_S \left(\frac{pp_4}{pp_{40}}\right)_{\text{RGA}} \left[1 - 0.11 \left(\frac{pp_4}{pp_{40}}\right)_{\text{RGA}}\right], \text{ small microcapillaries;} \tag{9}$$

where pp stands for the partial pressure reported by the RGA, $C_L \simeq 7.8$ and $C_S \simeq 8.0$. Based on a number of calibration runs, we suspect that systematic uncertainties in these values contribute about 1% to uncertainty in $(pp_4/pp_{40})_{\text{true}}$. The heavy mole fraction is then given by

$$n_H = \frac{1}{1 + (pp_4/pp_{40})_{\text{true}}}. \tag{10}$$

At the start of each experimental run (and at the end of the longest full-day runs), we

remeasured C_L and C_S with our 50–50 feedstock. These constants changed from day to day by up to 2%. However, we retained the nonlinear coefficient 0.11 in Eq. (9) for all experimental runs.

In laminar flow of an ideal gas, the mole flux through a circular capillary of diameter D from pressure p to zero pressure is obtained from[19]

$$-\frac{dp}{dx} = \frac{128\mu}{\pi D^4} U, \tag{11}$$

where $U = \dot{N} R_{\rm univ} T/p$ is the volume flow rate and μ is the viscosity. Integrating Eq. (11) from $x = 0$ at one end of the capillary to $x = \Delta x$ at the other shows that

$$\frac{[p(0)]^2 - [p(\Delta x)]^2}{2} = \mu \frac{128 \Delta x}{\pi D^4} \dot{N} R_{\rm univ} T \equiv \mu Z \ \dot{N} R_{\rm univ} T, \tag{12}$$

where $Z = 128\Delta x/\pi D^4$ includes the geometrical parts of the flow impedance. At the high-pressure end of a microcapillary, the mean free path is only about 1% of the diameter, so the gas should flow as a viscous fluid. However, $p(\Delta x) = 0$ at the low-pressure end, and the assumption of laminar flow is questionable because the mean free path exceeds the capillary diameter. The crossover to the molecular-flow regime, where the mean free path is of the order of the microcapillary diameter, occurs around $p = 0.01$ bar, approximately 5 μm from the low-pressure ends of the 5-cm long microcapillaries. Safely ignoring such a small fraction of the microcapillary length, Eq. (12) shows that $\dot{N} \propto [p(0)]^2$. This quadratic dependence was experimentally observed, using the argon partial pressure at the RGA as a proxy proportional to $\dot{N}$. (This proportionality depends on the assumptions that the volumetric pumping speed of argon through the turbo pump is independent of argon partial pressure, justified by the pump's specifications, and that the RGA's sensitivity to argon is approximately independent of partial pressure.)

Fittings at the top, middle, and bottom of the separation tube allowed connection of capillaries for feedstock injection and product removal. Figure 1 shows one such capillary at each of those three locations; other arrangements are discussed below as they arise. Each of these stainless-steel capillaries was nominally 127 μm (0.005 inch) inside diameter and 15 cm long. To obtain an accurate value of the geometrical factor Z for each capillary, we used an auxiliary setup in which we timed the displacement of a liquid out of an inverted graduated cylinder as feedstock gas with $n_H = 0.50$, driven by a known pressure, flowed steadily through the capillary into the graduated cylinder. A mixture of 90% glycerin, 10% water, and a few drops of food coloring provided low vapor pressure and not-too-high viscosity. Care was taken to avoid effects of surface tension and to account for the changing head of the liquid. Equation (12) and the time derivative of the ideal-gas law, $pU = \dot{N} R_{\mathrm{univ}} T$, were used to obtain Z from the measured pressures and volume flow rates. Five measurements were made with each capillary, with flow rates ranging from 1 to 5 μmol/s. No single determination of Z differed from the average for that capillary by 1%. We believe that systematic errors totalled at most 2%. (The measurements showed that the inside diameters of the capillaries were 5% to 6% larger than their nominal values.)

Later, during mixture-separation experiments, the mole fluxes into and out of the separation tube through these capillaries were controlled by needle valves[20] connected to the feedstock gas through a pressure regulator[21] and to a vacuum pump though an old, homemade rubber-membrane manostat.[22] The flow rates were determined via Eq. (12) by measurements of the pressures at the the ends of the capillaries using the piezoresistive transducers shown in Fig. 1 and knowledge of Z obtained as described in the previous paragraph. We accounted for the n_H and T dependences of the gas viscosity. We neglected acoustic streaming's contribution to the pressure difference[23] across the capillaries, $|p_1|^2 / 4p_m$, because it was only

0.04% to 1% of the pressure difference of Eq. (12) for all measurements.

Establishing a desired wave in the separation tube was an iterative procedure, carried out intermittently over a period of an hour or two as steady state was approached. We adopted a standard target of 3.00 kPa amplitude in the center of the tube, and a purely real acoustic impedance $z = Ap_1/U_1$ equal to $\rho_m a$ in the center of the tube to achieve a pure traveling wave there. We made a DeltaE model of the apparatus with these constraints and with the desired conditions of steady flow. The DeltaE model's complex p_1 at the two ends of the separation tube then served as goals to which experimental measurements could be compared, and adjustments to the complex voltages imposed on the two driver assemblies were made to bring the experimental p_1's close to their goals. This might seem to be a complicated procedure, because two experimental voltage amplitudes and two experimental voltage phases were being adjusted to try to meet two experimental pressure amplitudes and two experimental pressure phases. However, the overall time phase of the oscillation is a meaningless variable, and the overall amplitude of the wave was reliably changed by any desired fractional amount when the amplitudes of both drive voltages were changed by that same fractional amount. Thus, it was necessary only to measure changes in p_1 at the ends of the separation tube in response to two small changes: a small change in phase difference between the two driver voltages, and a small fractional increase in driver voltage at one driver. The matrix of these measurements was inverted to allow a prediction of the complex drive voltages needed to achieve desired p_1's. Two iterations might have sufficed to bring the wave close to the goal, but $n_H(x)$ was also evolving during the course of these iterations, changing the density and sound speed along the separation tube, so three or four iterations were usually needed.

To illustrate how well this wave–tune-up procedure was typically accomplished and to

establish confidence in the measurement techniques, Fig. 2 shows experimental and DeltaE results with no steady flow in the separation tube. Figure 2(a) compares the experimental and calculated pressure waves, with the zero of phase arbitrarily chosen to be the phase of the calculated p_1 at the middle of the separation tube. The agreement between the calculated and measured complex pressures at the two ends is indicative of how well the tune-up procedure described in the previous paragraph was routinely carried out, and the agreement between the calculated p_1 and measured p_1 at the middle of the separation tube is then one indication of how accurately we are modeling the wave. Figure 2(b) compares experimental and calculated mole fractions, and is a second indication of how accurately we are modeling the wave and its mixture-separation effects. The differences between measurements and calculations in Fig. 2(b) are about 1%, comparable to the expectations outlined above and similar to what was described in Ref. 3. Figure 2(c) shows calculations of specific acoustic impedance $z = p_1 A/U_1$ along the tube for this wave, showing how well this arrangement can maintain a purely traveling wave along its entire length, even while the acoustic power decreases from 0.19 W at $x = 0$ to 0.08 W at $x = 1$ m.

Imposing nonzero mole flux on the separation tube through the feedstock and product capillaries requires a small amount of additional, non-acoustic power to overcome the viscous impedances of the capillaries. In the present experiment, the ideal mechanical power required to isothermally compress the feedstock from 80 kPa to the feestock pressure and to isothermally compress the products from the product-suction pressure to 80 kPa can be taken as a fair measure of the extra power required. As an example from the high end of the range of flows discussed below, this power totals only 10 mW for 4 μmol/s flowing in through one feedstock capillary and 2 μmol/s flowing out through each of two product capillaries.

III. THERMOACOUSTICS IN CAPILLARIES

To accurately measure $n_H(x)$ with this apparatus, we must be assured that the concentration gradient in each microcapillary is small enough that n_H at the RGA does not differ significantly from n_H in the separation tube where the microcapillary is attached. To perform continuous separations, we must similarly be certain that dn_H/dx in the feedstock capillaries and product capillaries can be neglected, or at least is understood quantitatively. We must also know that acoustic power dissipation in the capillaries is acceptably small. In this section, we analyze these issues, using the small-radius limits of the mixture-separation results in the Appendix and other equations of thermoacoustics.

Ignoring the effects of steady flow, which will be discussed below, the wall-damped Helmholtz equation for pure gases is[9]

$$[1 + (\gamma - 1)\, f_\kappa]\, p_1 + \frac{a^2}{\omega^2}\,(1 - f_\nu)\,\frac{d^2 p_1}{dx^2} = 0, \tag{13}$$

with the viscous-dissipation function f_ν and the thermal-dissipation function f_κ in a circular tube of radius R given by

$$f_j = \frac{2J_1\left[(i-1)\,R/\delta_j\right]}{\left[(i-1)\,R/\delta_j\right] J_0\left[(i-1)\,R/\delta_j\right]}, \tag{14}$$

where J_n is the nth-order Bessel function, $\delta_\nu = \sqrt{2\mu/\omega\rho_m}$ is the viscous penetration depth, and $\delta_\kappa = \sqrt{2k/\omega\rho_m c_p}$ is the thermal penetration depth, and j is either ν or κ. For small R, Eq. (14) becomes

$$f_j \simeq 1 - \frac{i}{4}\frac{R^2}{\delta_j^2} - \frac{1}{12}\frac{R^4}{\delta_j^4} + O(R^6). \tag{15}$$

Substitution of Eq. (15) into Eq. (13) yields, to lowest order in R, the Helmholz equation for a small circular tube:

$$\left(1 - \frac{i}{4}\frac{\gamma - 1}{\gamma}\frac{R^2}{\delta_\kappa^2}\right) p_1 + \frac{i}{4}\frac{R^2}{\delta_\nu^2}\frac{a^2}{\gamma\omega^2}\frac{d^2 p_1}{dx^2} = 0. \tag{16}$$

The solution $p_1(x)$ to Eq. (16) is the sum of positive and negative complex exponentials of x. To conveniently satisfy boundary conditions at the ends of the capillary, the solution can be written in either of two forms,

$$p_1 = p_{1,0}e^{-\alpha x}, \text{ infinite length,} \tag{17}$$

$$p_1 = p_{1,0}\frac{\sinh\alpha\,(\Delta x - x)}{\sinh\alpha\Delta x}, \text{ finite length,} \tag{18}$$

for capillaries driven at $x = 0$ with a complex pressure amplitude $p_{1,0}$. The first form is for a capillary extending from $x = 0$ to infinity, and the second form is for a capillary of length Δx with $p_1 = 0$ at $x = \Delta x$. Substitution of either form into Eq. (16) and use of the general identity $a = \lambda f$ relating the sound speed a, the wavelength λ, and the frequency f shows that

$$\alpha^{-1} = \frac{1-i}{\sqrt{2}}\,\frac{1}{4\pi\sqrt{\gamma}}\frac{R}{\delta_\nu}\lambda \tag{19}$$

to lowest order in R. The volume flow rate U_1 is obtained from Eqs. (17)–(19) via[9]

$$U_1(x) = \frac{i\pi R^2\,(1-f_\nu)}{\omega\rho_m}\frac{dp_1}{dx} \tag{20}$$

$$\simeq -\frac{\pi}{8}\frac{R^4}{\mu}\frac{dp_1}{dx}. \tag{21}$$

For a gas mixture, f_κ in Eq. (13) should be replaced by a linear combination of $f_{\kappa D}$ and $f_{D\kappa}$, which are defined in Ref. 3. However, the absence of δ_κ from Eqs. (17)–(19) shows that this detail is irrelevant for the determination of α in the present problem.

Table I displays some numerical values for the gas, the microcapillaries, the feedstock/product capillaries, and the separation tube. In the microcapillaries, $\left|e^{-\alpha\Delta x}\right| = 2\times10^{-6}$, so Eq. (17) is appropriate. The feedstock/product capillaries have $\left|e^{-\alpha\Delta x}\right| = 0.06$, so Eq. (18) would be required for high accuracy, but for simplicity it is not used here.

To estimate the end-to-end concentration difference that develops in a capillary, we begin by considering Eq. (4). The two terms with dn_H/dx typically subtract from the $|p_1|\,|U_1|$

term and are smaller than it. Thus, $\dot{N}_H - n_H\dot{N}$ will never be much larger than the $|p_1|\,|U_1|$ term, and $\dot{N}_H - n_H\dot{N}$ can be neglected when estimating the order of magnitude of dn_H/dx in the capillary. In small enough tubes or at low enough amplitudes, the third term in Eq. (4) can be neglected in comparison to the fourth term, because their ratio,

$$\frac{\text{3rd term}}{\text{4th term}} = \frac{1}{16\pi}\frac{L}{\gamma\sigma}\frac{R\lambda^2}{\delta_\kappa^3}F_{\text{grad}}\frac{|p_{1,0}|^2}{p_m^2}e^{-2\,\text{Re}[\alpha]x} \tag{22}$$

is proportional to $R^4\,|p_{1,0}|^2$. (Note that F_{grad} is proportional to R^3 for small R.) To obtain Eq. (22) and subsequent results in this section, it is necessary to use Eqs. (21), (19), and (17), the definitions $\sigma = \delta_\nu^2/\delta_\kappa^2$ and $L = \delta_\kappa^2/\delta_D^2$ given in Ref. 3, and the ideal-gas identities $a^2 = \gamma R_{\text{univ}} T_m$ and $p_m = \rho_m R_{\text{univ}} T_m/m_{\text{avg}}$. Based on the numerical values in Table I for Eq. (22), we neglect the third term in Eq. (4).

With these approximations, Eq. (4) becomes

$$0 \simeq \frac{\delta_\kappa}{2R}\frac{\gamma-1}{\gamma}\frac{k_T}{R_{\text{univ}}T_m}\left(F_{\text{trav}}\cos\theta + F_{\text{stand}}\sin\theta\right)|p_1|\,|U_1| - N\pi R^2 D_{12}\frac{dn_H}{dx} \tag{23}$$

in a capillary. Solving this equation for dn_H/dx and integrating along the length of the capillary, using Eqs. (17)–(19) as necessary, with $\theta = 3\pi/4$ from Eqs. (17) and (21), and using the small-R limits of F_{trav} and F_{stand},

$$F_{\text{trav}} \;\propto\; R^5, \tag{24}$$

$$F_{\text{stand}} \;\simeq\; \frac{1}{12}\frac{R^3}{\delta_\kappa^3}, \tag{25}$$

yields finally

$$\Delta n_H \simeq \frac{1}{384\pi^2}\frac{(\gamma-1)\,L}{\gamma^2\sigma}k_T\frac{\lambda^2R^4}{\delta_\kappa^6}\frac{|p_{1,0}|^2}{p_m^2} \tag{26}$$

for infinite length. Numerical values are given in Table I, and are much smaller than the mole-fraction resolution of our apparatus.

The acoustic power consumed by each capillary can be calculated with

$$\dot{E}_2(0) = \frac{1}{2}\mathrm{Re}\left[p_1(0)\widetilde{U_1}(0)\right]. \tag{27}$$

Substituting Eq. (21) into Eq. (27) yields

$$\dot{E}_2 = \sqrt{\frac{\gamma}{32}}\frac{|p_{1,0}|^2}{\rho_m a}\pi R^2 \frac{R}{\delta_\nu} \tag{28}$$

for infinite length. Numerical values are given in Table I. Fortunately, these powers are negligible compared with the ~ 100 mW consumed in the separation tube.

In most of the circumstances of interest in this paper, the steady flow in the capillaries overwhelms the oscillating flow, invalidating the analysis above. At 1 μmol/s in a feedstock/product capillary, the steady flow equals the amplitude of the oscillating flow at the high-$|p_1|$ end of the capillary, and the capillary is swept clean by the steady flow in only 10 acoustic cycles. Thus, the analysis above is probably only valid for flows below about 0.1 μmol/s in the feedstock/product capillaries. However, it is hard to imagine how faster steady flows could *increase* the ability of the thermoacoustic phenomena to create a concentration gradient. In the microcapillaries, the steady flow is about twice the amplitude of the oscillating flow at the high-$|p_1|$ end.

Two microcapillaries (not shown in Fig. 1) leading to the RGA from the left ends of the two product capillaries shown in Fig. 1 were used to verify that the product streams indeed carried the same mole fractions as were observed in the separation tube at the product-capillary entrances.

IV. DISCUSSION OF THERMOACOUSTIC RESULTS

Figures 3, 4, and 5 show the heavy mole fraction in the separation tube under a variety of conditions of nonzero total mole flux of feedstock and product(s). In all cases, calculations

and measurements are in good agreement, confirming the presence of the $n_H\dot{N}$ term in Eq. (4) and our understanding of the boundary condition on n_H discussed near Eq. (6). It should be noted that there are no adjustable parameters in the calculations producing the curves in these figures. The calculations integrate Eq. (4), simultaneously with Eqs. (2) and (3), with respect to x, using the experimental values of $p_1(0)$, $p_1(x = 1\text{ m})$, frequency, mean pressure, $n_{H,\text{feedstock}}$, and $\dot{N}$ in each feedstock and product capillary, and with the boundary condition Eq. (6) imposed on n_H wherever product flows out of the separation tube.

Figure 3 shows n_H vs x for feedstock injection at $x = 0.5$ m. In Fig. 3(a), where half of the feedstock is removed at each end of the separation tube, the effect of simply increasing $\dot{N}$ in Eq. (4) is apparent: a reduction in the slope $|dn_H/dx|$ and an increase in the curvature of $n_H(x)$ as $\dot{N}$ is increased. These effects are analogous to the temperature slope changes and curvature seen in thermoacoustic refrigeration by Reid,[24–26] because $n_H\dot{N}$ and the terms with dn_H/dx in Eq. (4) here are mathematically identical in form to $\dot{m}c_pT_m$ and terms with dT_m/dx in the energy equation in Reid's work. To the extent that the implicit n_H and x dependences of all variables in Eq. (4) could be neglected, that equation would be of the form

$$\dot{N}_H = \alpha + \dot{N}n_H + \beta\frac{dn_H}{dx}, \tag{29}$$

where α and β can be regarded as constants, so $n_H(x)$ would have an exponential curvature.

Figure 3(b) is less symmetrical than Fig. 3(a) because 20% of the feedstock mole flux is removed at $x = 0$ and 80% at $x = 1$ m in Fig. 3(b). The slopes are shallower and the curvatures greater on the right half of the figure than on the left half because $\dot{N}$ is greater on the right half, as discussed in the previous paragraph. The heavy mole fraction at $x = 0.5$ m is different from $n_{H,\text{ feedstock}} = 0.50$, with the difference growing as the feedstock mole flux

decreases and exerts weaker local influence on $n_H(x)$.

Figure 4 illustrates most clearly the sometimes counterintuitive nature of the boundary condition for n_H expressed in Eq. (6). For the circles and squares, feedstock with $n_{H,\text{ feedstock}} = 0.50$ is injected at $x = 1$ m and all of the product is removed at $x = 0$. One might at first guess that n_H would be close to 0.50 at the feedstock end of the separation tube, but instead n_H is tied firmly to 0.50 at the *product* end of the separation tube. One way to interpret this result is to realize that, in steady state with only one feedstock capillary and one product capillary, what flows out of the product capillary must be exactly what flows in through the feedstock capillary, which has $n_H = 0.50$. In the context of Eq. (6), the product total mole flux and heavy mole flux must equal their values for the feedstock, so the product's n_H must also equal its value in the feedstock.

For Fig. 3(b), in which 20% of $\dot{N}_{\text{feedstock}}$ flows out at $x = 0$ and 80% at $x = 1$ m, corresponding global steady-state arguments show that

$$0.20\ n_H(0) + 0.80\ n_H(1.0\text{ m}) = n_{H,\text{ feedstock}} = 0.50, \tag{30}$$

which is indeed the case. The triangles in Fig. 4 also illustrate Eq. (30) for one feedstock and two product capillaries, though with different numerical values. In contrast to Fig. 3(b), in which the feedstock enters at the center of the separation tube and the two products are removed at the ends, the triangles in Fig. 4 represent a case in which the feedstock enters at one end and the two products are removed at the two ends.

Figure 5 shows how n_H in the two product streams at the ends of the separation tube varies with flow rate, when the feedstock is injected at the middle of the separation tube. Purities decrease with increasing flow rates, and the purity of one product can be enhanced by reducing the fraction of the feedstock that flows into it. For this separation tube running

with a 3-kPa traveling wave, product flow rates of the order of 1 to 10 μmol/s cause a significant decrease in purities.

V. CONCLUSIONS

Measurements confirm that the addition of the simple term $n_H\dot{N}$ to the thermoacoustic mixture-separation equation for the heavy mole flux $\dot{N}_H$ accounts for a nonzero total mole flux $\dot{N}$. The influence of $\dot{N}$ on $n_H(x)$ is similar to that of steady flow on $T_m(x)$ in the stack of a standing-wave refrigerator: The magnitude of the slope $|dn_H/dx|$ is reduced, and $n_H(x)$ acquires significant curvature, as $\dot{N}$ is increased. Measurements also show that a boundary condition constraining the solution $n_H(x)$ is imposed wherever steady flow leaves the separation tube and enters a small-diameter capillary with negligible thermoacoustic characteristics of its own. Flow out through such a capillary carries whatever mole fraction is present in the separation tube where the capillary is attached. No such boundary condition is imposed by feedstock entering the separation tube through such a small capillary.

Capillaries suitable for practical continuous thermoacoustic mixture separation have been demonstrated. Such capillaries are small enough in diameter that they do not develop significant internal concentration gradients, nor do they consume significant acoustic power. Nevertheless they are large enough to carry significant steady flow without prohibitively large steady pressure drops.

Acknowledgments

This work was supported by Locally Directed R&D funds at Los Alamos National Laboratory. We thank Scott Backhaus for helpful conversations and Mike Torrez for expert

layout and assembly of the apparatus.

APPENDIX: THERMOACOUSTIC MIXTURE SEPARATION IN CIRCULAR TUBES

The time-averaged mole flux of the heavy component is given by Eq. (4), where the dependences on the radius of the tube are in the three functions $F_{\rm trav}$, $F_{\rm stand}$, and $F_{\rm grad}$. Analytical expressions for the three F's in the boundary-layer limit have been published previously.[1,3] Here we present such expressions for circular tubes of arbitrarily small radius, starting from Eq. (3) and from Eqs. (47) and (48) of Ref. 3.

Unfortunately, Eq. (48) of Ref. 3 has a minus-sign typographical error; the correct expression is:

$$\begin{aligned}\dot{N}_{H,2} \;=\; & \frac{1}{2}\frac{\gamma-1}{\gamma}\frac{k_T/\varepsilon}{R_{\rm univ}T_m}\Re\left\{\frac{p_1\tilde{U}_1}{1-\tilde{f}_\nu}\left[C\left(\frac{\delta_\kappa^2}{\delta_{\kappa D}^2}-1\right)\left\langle h_{\kappa D}\left(1-\tilde{h}_\nu\right)\right\rangle\right.\right. \\ & +(1-B-C)\left(\frac{\delta_\kappa^2}{\delta_{D\kappa}^2}-1\right)\left\langle h_{D\kappa}\left(1-\tilde{h}_\nu\right)\right\rangle \\ & \left.\left.-B\frac{\sigma-1}{\sigma}\left\langle h_\nu\left(1-\tilde{h}_\nu\right)\right\rangle\right]\right\} \end{aligned} \tag{A.1}$$

where the last line here has the sign error fixed. B and C are given in Eqs. (33) and (34) of Ref. 3. Note that B is proportional to the concentration gradient and that C contains one term proportional to B and one term independent of the gradient. The $\langle\ \rangle$ above denotes the average over cross-sectional area, and

$$h_j = \frac{J_0\left[(i-1)\,r/\delta_j\right]}{J_0\left[(i-1)\,R/\delta_j\right]}, \tag{A.2}$$

where J_0 is the zeroth-order Bessel function and j is either ν or κ.

To evaluate averages of the form $\langle h_i(1-\tilde{h}_j)\rangle$, one can use identity (11.3.20) from Ref. 27:

$$\int_0^z t^\nu J_{\nu-1}(t)dt = z^\nu J_\nu(z) \quad \text{for} \quad \mathrm{Re}\left[\nu\right] > 0 \tag{A.3}$$

to verify that

$$\langle h_j \rangle = f_j. \tag{A.4}$$

Then one can use Ref. 27's Eq. (9.1.40)

$$\widetilde{J}_\nu(z) = J_\nu(\widetilde{z}) \tag{A.5}$$

and Eq. (11.3.29):

$$\begin{aligned}\int^z \left\{(k^2-l^2)t - \frac{(\mu^2-\nu^2)}{t}\right\} \mathcal{C}_\mu(kt)\mathcal{D}_\nu(lt)dt \;=\; & z\left\{k\mathcal{C}_{\mu+1}(kz)\mathcal{D}_\nu(lz) - l\mathcal{C}_\mu(kz)\mathcal{D}_{\nu+1}(lz)\right\} \\ & -(\mu-\nu)\mathcal{C}_\mu(kz)\mathcal{D}_\nu(lz),\end{aligned} \tag{A.6}$$

where $\mathcal{C}$ and $\mathcal{D}$ are any two cylindrical Bessel functions, to compute

$$\langle h_i \tilde{h}_j \rangle = \frac{\delta_j^2}{\delta_i^2+\delta_j^2} f_i + \frac{\delta_i^2}{\delta_i^2+\delta_j^2}\tilde{f}_j. \tag{A.7}$$

Combining Eqs. (A.4) and (A.7) yields the result needed in Eq. (A.1),

$$\langle h_i(1-\tilde{h}_j)\rangle = \frac{\delta_i^2}{\delta_i^2+\delta_j^2}(f_i - \tilde{f}_j), \tag{A.8}$$

and identification of expressions for the F's in Eq. (A.1) is straightforward. The results are

$$F_{\rm trav} \;=\; -\frac{R}{\delta_\kappa}{\rm Re}\left[\frac{G}{\left(1-\tilde{f}_\nu\right)}\right], \tag{A.9}$$

$$F_{\rm stand} \;=\; \frac{R}{\delta_\kappa}{\rm Im}\left[\frac{G}{\left(1-\tilde{f}_\nu\right)}\right], \tag{A.10}$$

$$\begin{aligned}F_{\rm grad} \;=\; & -\frac{R}{\delta_\kappa}\frac{1}{|1-f_\nu|^2}\frac{\sigma}{(1-\sigma)(1-\sigma L)-\varepsilon\sigma} \\ & {\rm Im}\left[\frac{(\sigma-1)}{\sigma S} f_\nu\left(\frac{\delta_\kappa^2-\delta_{\kappa D}^2}{\delta_\nu^2+\delta_{\kappa D}^2}f_{\kappa D} - \frac{\delta_\kappa^2-\delta_{D\kappa}^2}{\delta_\nu^2+\delta_{D\kappa}^2}f_{D\kappa} + \frac{(1+\sigma)\,LQ}{M}\tilde{f}_\nu + S\right) + \varepsilon G\right],\end{aligned} \tag{A.11}$$

where R is the circle radius and

$$S = \left(\frac{\delta_\kappa^2}{\delta_{D\kappa}^2} - 1\right) f_{D\kappa} - \left(\frac{\delta_\kappa^2}{\delta_{\kappa D}^2} - 1\right) f_{\kappa D}, \tag{A.12}$$

$$Q = \frac{\delta_{\kappa D}^2 - \delta_{D\kappa}^2}{\delta_\kappa^2}, \tag{A.13}$$

$$M = (1+\sigma)(1+\sigma L) + \varepsilon\sigma, \tag{A.14}$$

$$G = \frac{\sigma L Q}{MS} f_{\kappa D} f_{D\kappa} + \frac{\tilde{f}_\nu}{S}\left(\frac{f_{\kappa D}}{1+\delta_\nu^2/\delta_{D\kappa}^2} - \frac{f_{D\kappa}}{1+\delta_\nu^2/\delta_{\kappa D}^2}\right). \tag{A.15}$$

---

* Electronic address: swift@lanl.gov; URL: www.lanl.gov/thermoacoustics/

[1] G. W. Swift and P. S. Spoor. Thermal diffusion and mixture separation in the acoustic boundary layer. *J. Acoust. Soc. Am.*, 106:1794–1800, 1999. Errata J. Acoust. Soc. Am. 107:2299, 2000; 109:1261, 2001.

[2] P. S. Spoor and G. W. Swift. Thermoacoustic separation of a He–Ar mixture. *Phys. Rev. Lett.*, 85:1646–1649, 2000.

[3] D. A. Geller and G. W. Swift. Saturation of thermoacoustic mixture separation. *J. Acoust. Soc. Am.*, 111:1675–1684, 2002.

[4] D. A. Geller and G. W. Swift. Thermodynamic efficiency of thermoacoustic mixture separation. *J. Acoust. Soc. Am.*, 112:504–510, 2002.

[5] D. A. Geller and G. W. Swift. Thermoacoustic enrichment of the isotopes of neon. *J. Acoust. Soc. Am.*, 115:2059–2070, 2004.

[6] R. W. Rousseau, ed. *Handbook of Separation Process Technology.* Wiley, 1987.

[7] D. M. Ruthven, ed. *Encyclopedia of Separation Technology.* Wiley, 1997.

[8] S. Villani. *Isotope Separation.* American Nuclear Society, La Grange Park IL, 1976.

[9] G. W. Swift. *Thermoacoustics: A Unifying Perspective for some Engines and Refrigerators*. Acoustical Society of America Publications, Sewickley PA, 2002.

[10] W. C. Ward and G. W. Swift. Design environment for low amplitude thermoacoustic engines (DeltaE). *J. Acoust. Soc. Am.*, 95:3671–3672, 1994. Software and user's guide available either from the Los Alamos thermoacoustics web site www.lanl.gov/thermoacoustics/ or from the Energy Science and Technology Software Center, US Department of Energy, Oak Ridge, Tennessee.

[11] MKS Baratron Type 390HA, www.mksinst.com.

[12] Endevco, San Juan Capistrano, CA, www.endevco.com.

[13] Model SR830, Stanford Research Systems, Sunnyvale CA, www.srsys.com.

[14] Polymicro Technologies LLC, www.polymicro.com.

[15] RGA 100, Stanford Research Systems, Sunnyvale CA, www.srsys.com.

[16] Turbo-V 70D, Varian Inc. Vacuum Technologies, www.varianinc.com.

[17] Dry Scroll Vacuum Pump SH-110, Varian Inc. Vacuum Technologies, www.varianinc.com.

[18] M. G. Rao and C. Dong. Evaluation of low cost residual gas analyzers for ultrahigh vacuum applications. *J. Vac. Sci. Technol. A*, 15:1312–1318, 1997.

[19] R. W. Fox and A. T. McDonald. *Introduction to Fluid Mechanics*. Wiley, 1985.

[20] Model S, Swagelok Inc., www.swagelok.com.

[21] Model PRG101, Omega Engineering, Stamford Connecticut. www.omega.com.

[22] M. Escorne and A. Mauger. Temperature control for liquid-helium cryostats below 4.2 K. *Rev. Sci. Instrum.*, 54:1693–1696, 1983.

[23] B. L. Smith and G. W. Swift. Measuring second-order time-average pressure. *J. Acoust. Soc. Am.*, 110:717–723, 2001.

[24] R. S. Reid, W. C. Ward, and G. W. Swift. Cyclic thermodynamics with open flow. *Phys. Rev. Lett.*, 80:4617–4620, 1998.

[25] R. S. Reid and G. W. Swift. Experiments with a flow-through thermoacoustic refrigerator. *J. Acoust. Soc. Am.*, 108:2835–2842, 2000.

[26] R. S. Reid. *Open cycle thermoacoustics*. PhD thesis, Georgia Institute of Technology, School of Mechanical Engineering, 1999.

[27] M. Abramowitz and I. E. Stegun. *Handbook of Mathematical Functions with Formulas, Graphs, and Mathematical Tables*. National Bureau of Standards, US Government Printing Office, Washington DC, 1964.

Table I. Properties of 50–50 helium–argon at 80 kPa, 300 K, and 200 Hz, and values for three tubes filled with that gas. The last three rows of the table are for $|p_{1,0}| = 2$ kPa.

	Microcapillary	Capillary	Separation tube
δ_ν	0.23 mm	← same	← same
δ_κ	0.36 mm	← same	← same
δ_D	0.39 mm	← same	← same
R	0.005 mm	0.064 mm	1.67 mm
$\lvert\alpha\rvert^{-1}$	3 mm	37 mm	
Δx	50 mm	150 mm	1000 mm
λ	2180 mm	← same	← same
F_{trav}	-9.43×10^{-12}	-5.48×10^{-6}	-0.345
F_{stand}	1.59×10^{-7}	4.58×10^{-4}	-0.047
F_{grad}	-7.11×10^{-8}	-2.05×10^{-4}	-0.210
Eq. (22) at $x = 0$	-6×10^{-7}	-0.02	
$\lvert\Delta n_H\rvert$	1×10^{-8}	3×10^{-4}	
$\dot{E}_2$	5 nW	10 μW	

FIGURE CAPTIONS

Figure 1. Scale drawing of the apparatus. Valves to the right of the drawing, not shown, connected the microcapillaries to the RGA and pumps. Valves to the left of the drawing, not shown, connected the feedstock/product capillaries to the source of gas and other pumps.

Figure 2. Results with no time-averaged total mole flux, plotted as a function of location x along the separation tube. Curves are calculations and points are experimental values. (a) Complex pressure. (b) Heavy mole fraction. (c) Specific acoustic impedance z compared with $\rho_m a$. Upper dashed curve is Re[z] and lower dashed curve is Im[z]. Solid curve near Re[z] is $\rho_m a$.

Figure 3. Heavy mole fraction n_H as a function of location x, for feedstock injected at $x = 0.5$ m and products removed at $x = 0$ and $x = 1$ m. Points are experimental values and associated curves are calculations. (a) Product mole fluxes equal. Circles, feedstock $\dot{N} = 3.96$ μmol/s. Squares, 0.99 μmol/s. Triangles, 0.26 μmol/s. (b) Product mole flux at $x = 0$ is 25% of product mole flux at $x = 1$ m. Circles, feedstock $\dot{N} = 3.63$ μmol/s. Squares, 1.59 μmol/s.

Figure 4. Heavy mole fraction n_H as a function of location x, for feedstock injected at one end and products removed at one or both ends. Points are experimental values and associated curves are calculations. Circles, 1.13 μmol/s injected at $x = 1$ m and removed at $x = 0$. Squares, 0.21 μmol/s injected at $x = 1$ m and removed at $x = 0$. Triangles, 3.36 μmol/s injected at $x = 1$ m, 2.88 μmol/s removed at $x = 1$ m, and 0.43 μmol/s removed at $x = 0$.

Figure 5. Heavy mole fraction n_H at $x = 0$ (points and curves above $n_H = 0.5$) and at $x = 1$ m (points and curves below $n_H = 0.5$) as a function of product mole flux rate at

$x = 0$. Feedstock is injected at $x = 0.5$ m and removed at $x = 0$ and $x = 1$ m. Points are experimental values and associated curves are calculations. Circles, feedstock flow equal to twice the $x = 0$ product flow. Squares, feedstock flow equal to five times the $x = 0$ product flow.

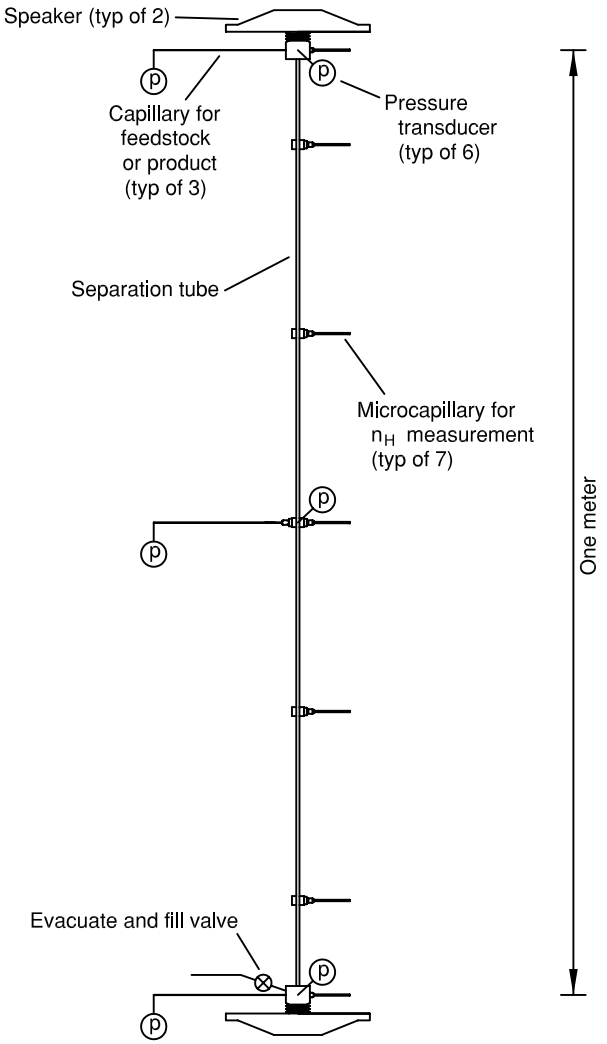

Figure 1
Swift and Geller
J. Acoust. Soc. Am.

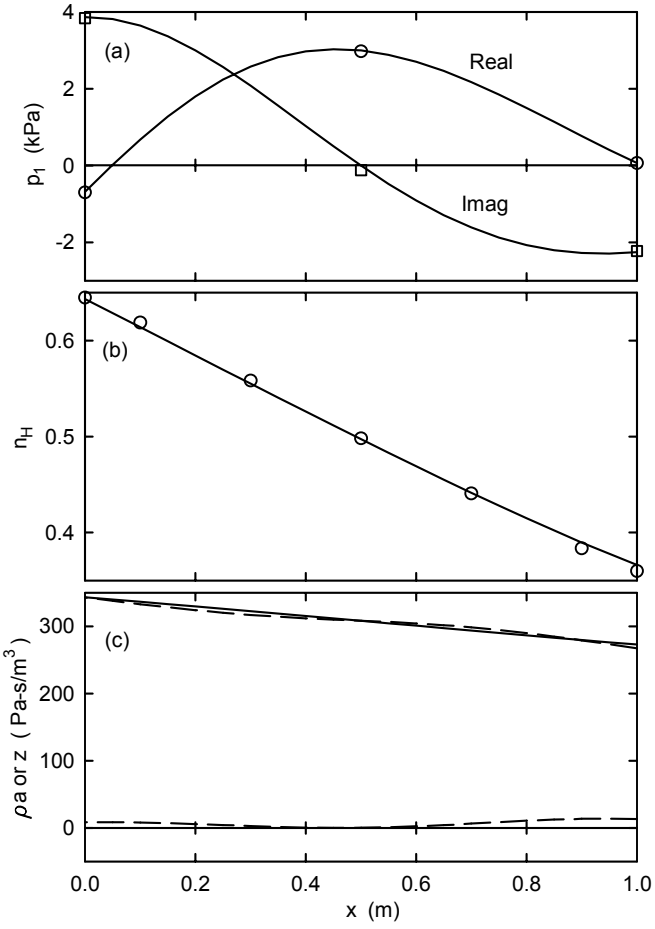

Figure 2
Swift and Geller
J. Acoust. Soc. Am.

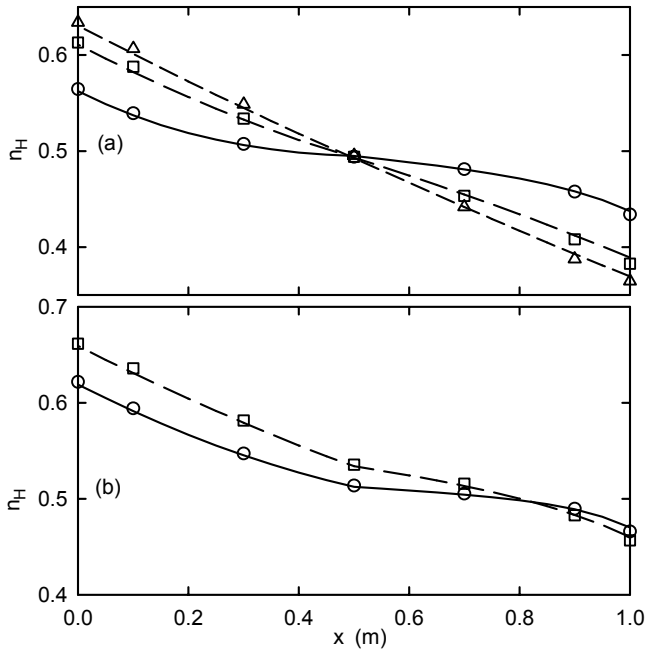

Figure 3
Swift and Geller
J. Acoust. Soc. Am.

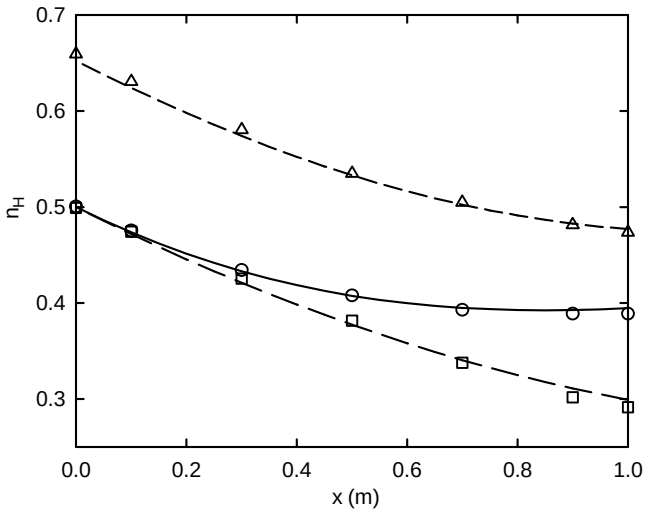

Figure 4
Swift and Geller
J. Acoust. Soc. Am.

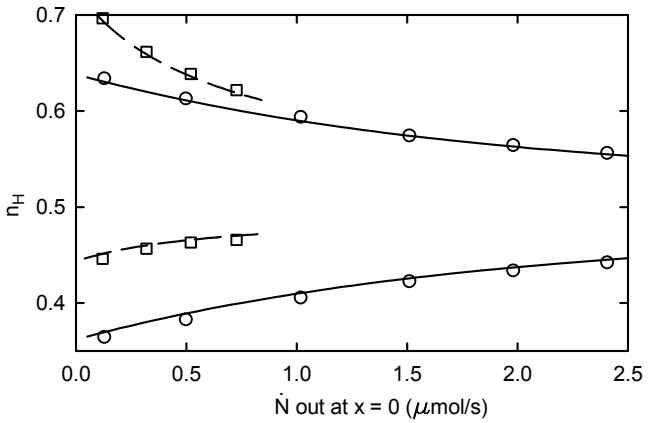

Figure 5
Swift and Geller
J. Acoust. Soc. Am.